Spatial free plastic forming of slender parts—numerical approaches for strain-hardening material

M Thalmair[1] and **H Lippmann**[2*]
[1]AGCO GmbH and Company KG, Marktoberdorf, Germany
[2]Lehrstuhl für Werkstoffkunde und Werkstoffmechanik, Technische Universität München, Garching, Germany

Abstract: A new metal forming process is described in which a slender part may be brought to a prescribed final shape by means of an appropriate, pre-calculated motion of its free ends only. Corresponding calculation schemes are presented for elastic/plastic material with strain hardening, and these are illustrated by practical examples.

Keywords: metal forming, plasticity, bending, torsion, theory, experiment, numerical methods

NOTATION

a	length of the rod
A	point on the central trajectory: left end (support)
b	generalized bending (component)
B	point on the central trajectory: right end (support)
C	point on the central trajectory: arbitrary
$\mathrm{d}(\mathbf{Q}, \zeta)$	multiplier function for plastic deformation in the elastic/plastic constitutive law
$\overline{d}$	generalized equivalent strain
$\mathbf{d}$, d	column matrix, component of generalized strain
D	point on the central trajectory: rear of the plastic zone
$\underline{\boldsymbol{e}}$, e	unit vector, component
$\overline{f}(\mathbf{Q}), f(\mathbf{Q})$	generalized yield criterion, yield potential
$\mathbf{F}$, F	column matrix, component of the force on the cross-section
$g(\mathbf{q})$	complementary yield potential
$\mathbf{K}$, K	compliance matrix, element
m	coefficient of the yield curve function
$\mathbf{M}$, M	column matrix, component of the generalized moment on the cross-section: in particular the bending moment
n	coefficient of the yield curve function
N	normal force acting on the cross-section
O	origin of coordinates fixed in space
P	point on the central trajectory: front of the plastic zone
$\mathbf{q}$, q	column matrix, component of generalized strain
$\mathbf{Q}$, Q	column matrix, component of the generalized stress on the cross-section
$\boldsymbol{r} = \mathbf{OC}$, r	radius vector, component
R	distance from the cone axis
s	arc length
t	time
T	torque on the cross-section
V	transversal force on the cross-section
$\mathbf{W}$, W	column matrix, coordinate of the virtual angular velocity
$\overline{Y}$	generalized yield limit: in particular the limit torque
α	scalar
$\alpha, \overline{\alpha}$	inclination angles of the conical spiral
γ	generalized shear (component)
Δ	denoting an increment in the subsequent quantity, for instance $\Delta\zeta^{\mathrm{D}}$
$\boldsymbol{\varepsilon}, \varepsilon$	column matrix, coordinate of the generalized longitudinal or shear strain: in particular the tension/compression normal to the cross-section
ζ	material longitudinal coordinate of the central trajectory
θ	mathematical torsion of the central trajectory
$\boldsymbol{\vartheta}, \vartheta$	column matrix, coordinate of the generalized bending and twist: in particular the torsion
Λ	rate of work per unit initial length

The MS was received on 9 June 2003 and was accepted after revision for publication on 17 December 2003.
* *Corresponding author: Lehrstuhl für Werkstoffkunde und Werkstoffmechanik, Technische Universität München, Boltzmannstrasse 15, D-85748 Garching, Germany.*

ρ	apex angle of the cone
φ	rotation angle around the inward normal to the cone

Subscripts

i, j, k	referring to material bases fixed to the cross-section, or counting components of the generalized stress/strain = 1, 2, 3
j', k', l'	counting components of the generalized stress/strain = 1, . . . , 6
L	referring to the plastic limit state
t	referring to the tangent of the central trajectory
κ, λ	referring to the basis fixed in space = x, y, z

Superscripts

A, B, C, D, O, P	referring to the corresponding points
e	referring to elastic deformation
p	referring to plastic deformation
0	referring to the initial time or value
∞	referring to the terminal state of the forming process
*	referring to the terminal position of D, for example, to the rear of a permanent plastically undeformed zone

1 INTRODUCTION

The elementary plane bending process in which a slender part is gripped at both its ends by hands or by appropriate tools, the motion of which leads to the generation of the final shape, has been further developed in several investigations (cf. references {**1**} and {**2**}) towards a new industrial forming process. The motions of the clamping tools are calculated in advance using an associated PC and are then fed into the control of the machine drives. In this way a large number of prescribed final shapes could be produced with fairly good accuracy, and the reproduction accuracy is even better. The lumped-mass approach presented in reference {**3**} opens up an alternative way to pre-calculate the motion of the clamping tools in particular under conditions of dynamics, although it is currently still confined to the primary problem (inverse to the one to be treated below) where the motion of the end cross-sections is prescribed while the final shape is searched for.

The generalization of the new metal forming process to spatial forming has been theoretically proposed in reference {**4**} and practically tested in reference {**5**}, although this process is still under investigation. For instance, the numerical integration scheme for the basic differential equations proposed in reference {**4**} is based on an incremental approach unfortunately demanding a numerical time differentiation. This may become a source of numerical error, and so a finite scheme was used instead, although still without detailed description in reference {**5**}. Such a finite constitutive law may be physically less correct than the incremental approach. However, besides reduced numerical effort, it also leads to a reduced numerical fluctuation because there is, in contrast to the incremental procedure, no error accumulation at the consecutive time steps. For plane bending, the finite scheme proved as sufficient anyway {**2**}. Therefore, in the present paper the still missing description of the finite integration scheme for spatial forming will be presented. Moreover, this scheme can also be applied successively in order to simulate the time steps of an incremental approach. Based on the finite scheme, the spatial forming process will be illustrated by two examples, i.e. a similarly bent and twisted bar of rectangular cross-section and a conical spiral of circular cross-section.

The integration methods to be developed are non-standard in the following sense. Although the initial shape and the final shape of the rod, i.e. the initial and the final distributions of displacement and of rotation of the cross-sections, are prescribed, the corresponding distribution of the external load is not of primary interest. On the contrary, the side condition holds, i.e. that there must not be any load distributed along the part. Actually, external loads are allowed at the end supports only. However, for these supports a complete *motion history* has to be found, bringing the part into the desired shape without any load acting at other places. From previous publications {**1**, **2**, **4**, **5**} it is clear that this motion history has to be based on a plastic zone moving from one end of the part, to be called A, towards the other end, B, thus leaving the plastically finished region of the part behind, while the plastically still undeformed region is in front of the moving zone. This zone shrinks to one single cross-section representing a *plastic hinge* if the generalized yield limit, $\overline{Y}$, is constant (*ideal* plasticity).

Subsequently it will be shown how this model can be transformed into an adequate numerical scheme. Unfortunately, a precise characterization of the possible shapes thus attainable is not known as yet. However, experience shows that a large variety of corresponding parts can be produced, provided the length is limited in order to avoid re-plastification of the already finished zone. A check of this situation has also to be included in the software, while other forming defects such as buckling of preferably thin-walled rods, or the deformation of the cross-sections in general, will not be discussed in this paper.

2 BASIC EQUATIONS

The slender part under consideration, briefly referred to as the *rod*, will be represented by a central trajectory AB

consisting of points C and the corresponding cross-sections, of which C is generally the geometrical centre of gravity. Although in the forming machine generally both clamping tools are driven {5}, it is for theoretical considerations sufficient to examine a cantilever with the rigid support at A and the free end at B (Fig. 1). Then the correct clamping in the machine requires no more than a superimposed rigid body transformation. Here, s represents the arc length (initially s^0), a is the total length (initially a^0) and ζ is a material coordinate in the constant limits, i.e. $\zeta^A \leqslant \zeta \leqslant \zeta^B$. The unit vectors $\boldsymbol{e}_1$, $\boldsymbol{e}_2$, $\boldsymbol{e}_3$ form a Cartesian tripod fixed to each cross-section such that $\boldsymbol{e}_1$ points in the normal direction towards growing s or ζ, while $\boldsymbol{e}_2$ and $\boldsymbol{e}_3$ define the orientation of the cross-section (*accompanying* tripod). Moreover, there are Cartesian base vectors $\boldsymbol{e}_x$, $\boldsymbol{e}_y$, $\boldsymbol{e}_z$ fixed in the space with origin O. Correspondingly, various sets of subscripts are introduced, i.e.

$$\begin{aligned} &i,j,k = 1,2,3, \qquad j',k',l' = 1,2,\ldots,6 \\ &\kappa,\lambda,\ldots = x,y,z \end{aligned} \tag{1}$$

As in reference {4}*, the partial derivatives with respect to time t or to the material longitudinal coordinate of the central trajectory, ζ, will be denoted by $^\bullet$ or by $'$ respectively, and the summation convention will be applied. Then, the radius vector, $\boldsymbol{r} = \mathbf{OC}$, the unit tangent vector, $\boldsymbol{e}_\mathrm{t}$, and the arc length, $s(\zeta)$, obey the conditions

$$\begin{aligned} &\boldsymbol{r} = r_\lambda \boldsymbol{e}_\lambda, \qquad s' = |\boldsymbol{r}'| > 0 \\ &\boldsymbol{e}_\mathrm{t} = \frac{\mathrm{d}\boldsymbol{r}}{\mathrm{d}s} = \boldsymbol{r}'/s' = (r'_\kappa/s')\boldsymbol{e}_\kappa \end{aligned} \tag{2}$$

The *virtual* angular velocity of the material cross-sections, $\mathbf{W}$, possessing the coordinates W_j with respect to the local base $\boldsymbol{e}_j$, is related to an observer, moving with the *virtual* velocity $\zeta' = 1$ along the then *virtually* rigid rod. Therefore, if $\varepsilon_{ijk} = \pm 1$ denotes the permutation tensor

$$\begin{aligned} &\boldsymbol{e}'_j = \mathbf{W} \times \boldsymbol{e}_j = \varepsilon_{ijk} W_i \boldsymbol{e}_k \qquad \text{where } \boldsymbol{e}_j = e_{j\kappa}\boldsymbol{e}_\kappa \\ &\boldsymbol{e}_\mathrm{t} = e_j \boldsymbol{e}_j = e_j e_{j\kappa} \boldsymbol{e}_\kappa \end{aligned} \tag{3}$$

e_j or $e_{j\kappa}$ being the coordinates of $\boldsymbol{e}_\mathrm{t}$ or $\boldsymbol{e}_j$ with respect to the bases $\boldsymbol{e}_j$ or $\boldsymbol{e}_\kappa$ respectively. For a finite integration scheme the generalized stress and strain are introduced

* Erratum to reference {4}: replace w'_k, v'_k, ω'_k and $w^\bullet_k$ with $(w')_k, (v')_k, (\omega')_k$ and $(w^\bullet)_k$ respectively at the first possible positions in equations (3), (4), (5), (7), (9) and (12), at the last possible position on p. 1855, line 12 from the bottom, and twice on p. 1855, line 7 from the bottom.

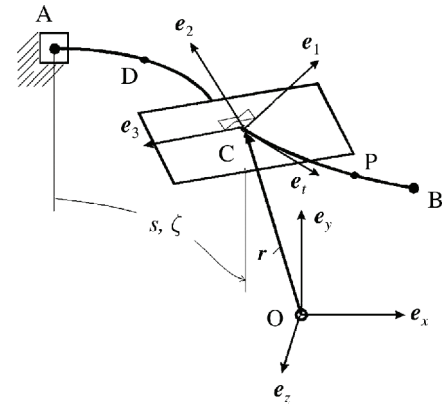

Fig. 1 Central trajectory of slender part AB with arbitrary point C and material cross-section, here rectangular. DP is the plastic zone moving from support A to B. The size and obliqueness of the cross-section are exaggerated for the sake of clarity

according to

$$\begin{aligned} \mathbf{Q} &= [Q_1, Q_2, \ldots, Q_6]^\mathrm{T} = [\mathbf{M}, \mathbf{F}]^\mathrm{T} = [M_1, M_2, M_3, F_1, F_2, F_3]^\mathrm{T} \\ &= [T, M_2, M_3, N, V_2, V_3]^\mathrm{T} \\ \mathbf{d} &= [d_1, d_2, \ldots, d_6]^\mathrm{T} = [\boldsymbol{\vartheta}, \boldsymbol{\varepsilon}]^\mathrm{T} = [\vartheta_1, \vartheta_2, \vartheta_3, \varepsilon_1, \varepsilon_2, \varepsilon_3]^\mathrm{T} \\ &= [\vartheta, b_2, b_3, \varepsilon, \gamma_2, \gamma_3]^\mathrm{T} \end{aligned}$$

where the superscript T denotes transposition, $F_1 = N$ and $F_2 = V_2, F_3 = V_3$ denote the resultant normal and transversal forces, $M_1 = T$ and M_2, M_3 denote the resultant torque and the bending moments, $\varepsilon_1 = \varepsilon$ is the local tension, $\varepsilon_2 = \gamma_2$ and $\varepsilon_3 = \gamma_3$ are the shear components, $\vartheta_1 = \vartheta$ denotes the torsion and $\vartheta_2 = b_2$ and $\vartheta_3 = b_3$ denote bending. If the rate of work, $\Lambda = \mathbf{Q}^\mathrm{T}\mathbf{d}^\bullet$, is related to rod elements of given initial length $\mathrm{d}s^0$ rather than to the actual length $\mathrm{d}s$, the strain rates deduced in reference {4} have to be multiplied by $\mathrm{d}s/\mathrm{d}s^0 = s'/s^{0\prime}$ to yield

$$\vartheta^\bullet_k = \frac{W^\bullet_k}{s^{0\prime}}, \qquad \varepsilon^\bullet_k = \frac{(s' e_k)^\bullet}{s^{0\prime}} \tag{4}$$

Then they become easily integrable with respect to time t to yield

$$\vartheta_k = \frac{W_k - W^0_k}{s^{0\prime}}, \qquad \varepsilon_k = \frac{s' e_k - s^{0\prime} e^0_k}{s^{0\prime}} \tag{5a}$$

or

$$\vartheta^\mathrm{e}_k = \frac{W_k - W^\infty_k}{s^{0\prime}}, \qquad \varepsilon^\mathrm{e}_k = \frac{s' e_k - s^{\infty\prime} e^\infty_k}{s^{0\prime}} \tag{5b}$$

where the superscript 0 refers to the initial state at time t^0, the superscript ∞ refers to the end of the forming process after final unloading and the superscript e refers to the elastic deformation superimposed on the plastic deformation, the latter to be identified by means of the superscript p. Actually, the forming process starts with elastic–plastic loading from the initial state {equation (5a)}, while final unloading is assumed to be purely

elastic {equation (5b)}. Equilibrium along the rod is expressed similarly to the equation two lines after (11) in reference {4} in terms of

$$M_k' + \varepsilon_{ijk}(W_i M_j + s' e_i F_j) + s^{0\prime} m_k = 0 \tag{6}$$

$$F_k' + \varepsilon_{ijk} W_i F_j + s^{0\prime} p_k = 0 \tag{7}$$

where the force or moment distributions, p_k or m_k, now per unit initial length rather than per unit actual length, may generally be disregarded under metal forming conditions. The column matrices of total strain will be decomposed into an elastic part and a plastic part regarding (1) according to

$$\mathbf{d} = \mathbf{d}^{\mathrm{e}} + \mathbf{d}^{\mathrm{p}} = [d_{j'}^{\mathrm{e}}]^{\mathrm{T}} + [d_{j'}^{\mathrm{p}}]^{\mathrm{T}} \tag{8}$$

The generalized Hooke's law will be assumed to hold for the elastic part

$$\mathbf{d}^{\mathrm{e}} = \mathbf{K}\mathbf{Q}, \qquad \text{where } \mathbf{K} = [K_{j'k'}] = [K_{k'}] = \mathbf{K}^{\mathrm{T}} \tag{9}$$

where $\mathbf{K}$ is the usual compliance matrix of the elastic rod. Regarding the plastic part, the generalized *equivalent strain increment*, $\overline{d} - \overline{d}^{\,0} = g(\mathbf{d}^{\mathrm{p}})$, is introduced, where $\overline{d}^{\,0}$ is the initial distribution of equivalent strain. Moreover, the *flow potential* $f = f(\mathbf{Q})$ and the *yield criterion* $\overline{f} = \overline{f}(\mathbf{Q})$ are considered. All of these functions are mathematically homogeneous {6}, obeying the relations

$$\begin{aligned}
&\overline{f}(\alpha\mathbf{Q}) = |\alpha|\overline{f}(\mathbf{Q}) > 0, \qquad f(\alpha\mathbf{Q}) = |\alpha| f(\mathbf{Q}) > 0\\
&g(\alpha\mathbf{d}^{\mathrm{p}}) = |\alpha|\, g(\mathbf{d}^{\mathrm{p}}) > 0\\
&g\left(\frac{\partial f}{\partial Q_{j'}}\right) \equiv f\left(\frac{\partial g}{\partial q_{j'}^{\mathrm{p}}}\right) \equiv 1 \qquad \text{if } \mathbf{Q} \neq \mathbf{0}, \mathbf{d}^{\mathrm{p}} \neq \mathbf{0}, \alpha \neq 0
\end{aligned} \tag{10}$$

in which α is a scalar and g is uniquely determined via the last identity by f, or vice versa, provided the functions are continuously differentiable with a non-vanishing gradient

$$\frac{\partial f}{\partial Q_{j'}} \neq \mathbf{0}, \qquad \frac{\partial g}{\partial q_{j'}^{\mathrm{p}}} \neq \mathbf{0}$$

everywhere, and if the hypersurfaces in the $\mathbf{Q}$-space or in the $\mathbf{q}$-space respectively, i.e. $\overline{f}(\mathbf{Q}) = \text{constant}$, $f(\mathbf{Q}) = \text{constant}$ and $g(\mathbf{q}) = \text{constant}$, are strictly convex; the first of these is the generalized *yield surface*. Then the generalized yield condition, the generalized finite flow rule and its inverse may be expressed in terms of

$$\begin{aligned}
&\overline{f}(\mathbf{Q}) = \overline{Y}(\overline{d}, \zeta), \qquad d_{j'}^{\mathrm{p}} = (\overline{d} - \overline{d}^{\,0})\frac{\partial f}{\partial Q_{j'}}\\
&Q_{j'} = f(\mathbf{Q})\frac{\partial g}{\partial d_{j'}^{\mathrm{p}}}
\end{aligned} \tag{11}$$

$\overline{Y} \geqslant 0$ being the generalized yield limit, the temperature dependence of which is not explicitly considered; $\overline{Y}$ may, for instance, be chosen as a limit bending or torsion moment. Here, $\overline{d}^{\,0}$ represents a possible prestrain so that $\overline{d}^{\,0} = 0$ at a virgin rod. Because of strain hardening, $\overline{Y}$ is strictly monotonically growing as a function of $\overline{d}$, so that $\overline{Y}$ may uniquely be inverted in terms of the function $\overline{d}(\overline{Y}, \zeta)$, from which another function $\mathrm{d}(\mathbf{Q}, \zeta)$ will be constructed according to

$$\begin{aligned}
&\mathrm{d}(\mathbf{Q}, \zeta) = \overline{d}(\overline{Y}, \zeta) - \overline{d}^{\,0} = \overline{d}(\overline{f}(\mathbf{Q}), \zeta) - \overline{d}^{\,0} \geqslant 0\\
&\quad \text{if } \overline{Y}(\overline{d}^{\,0}, \zeta) \leqslant \overline{f}(\mathbf{Q}) \text{ (plastic state)}\\
&\mathrm{d}(\mathbf{Q}, \zeta) = 0\\
&\quad \text{if } \overline{f}(\mathbf{Q}) < \overline{Y}(\overline{d}^{0}, \zeta) \text{ (elastic state)}
\end{aligned} \tag{12}$$

Then the finite elastic/plastic constitutive law may be written, observing (8), (10) and (12), as

$$\mathbf{d} = \mathbf{K}\mathbf{Q} + \mathrm{d}(\mathbf{Q}, \zeta)\frac{\partial f(\mathbf{Q})}{\partial \mathbf{Q}} \tag{13}$$

As $\mathbf{d}$ has been defined observing equations (5) in different ways for the loading and the unloading state, the latter is also covered by equation (13). Conversely, if a plastic state of strain $\mathbf{d}^{\mathrm{p}} \neq \mathbf{0}$ is known, the generalized stress $\mathbf{Q}$ follows from equations (10) and (11) according to

$$\begin{aligned}
Q_{l'} &= \frac{f(\mathbf{Q})}{\overline{f}(\mathbf{Q})}\overline{f}(\mathbf{Q})\frac{\partial g(\mathbf{d}^{\mathrm{p}})}{\partial d_{l'}^{\mathrm{p}}}\\
&= \frac{f(\partial g/\partial d_{k'}^{\mathrm{p}})}{\overline{f}(\partial g/\partial d_{k'}^{\mathrm{p}})}\overline{Y}(\overline{d}, \zeta)\frac{\partial g(\mathbf{d}^{\mathrm{p}})}{\partial d_{l'}^{\mathrm{p}}}\\
&= \frac{\overline{Y}(\overline{d}, \zeta)}{\overline{f}(\partial g/\partial d_{k'}^{\mathrm{p}})}\frac{\partial g(\mathbf{d}^{\mathrm{p}})}{\partial d_{l'}^{\mathrm{p}}}
\end{aligned} \tag{14}$$

3 INTEGRATION SCHEMES

Figure 2 represents a typical flowchart. The initial geometry of the rod may, for instance, be given by means of the following quantities, the values of which refer, just as an example, to an initially straight rod according to

$$\begin{aligned}
&W_i^0 \equiv 0, \qquad e_1^0 \equiv 1, \qquad e_2^0 \equiv e_3^0 \equiv 0, \qquad s^{0\prime} \equiv a^0\\
&e_{j\kappa} = 1 \qquad \text{if } j = 1, \kappa = x \text{ or } j = 2, \kappa = y\\
&\qquad\qquad \text{or } j = 3, \kappa = z,\\
&e_{j\kappa} = 0 \qquad \text{otherwise}
\end{aligned} \tag{15}$$

while the final geometry may be prescribed in terms of the distributions of $\mathbf{W}^{\infty}$ and $s^{\infty\prime}\mathbf{e}^{\infty}$, i.e. of $\mathbf{d}^{\infty}$ {cf. equations (5)}. In order to obtain a sufficient amount of control data for the machine drives, the integration has to be carried out with a sufficient number of time steps, although each of these steps is finite, i.e. related to the

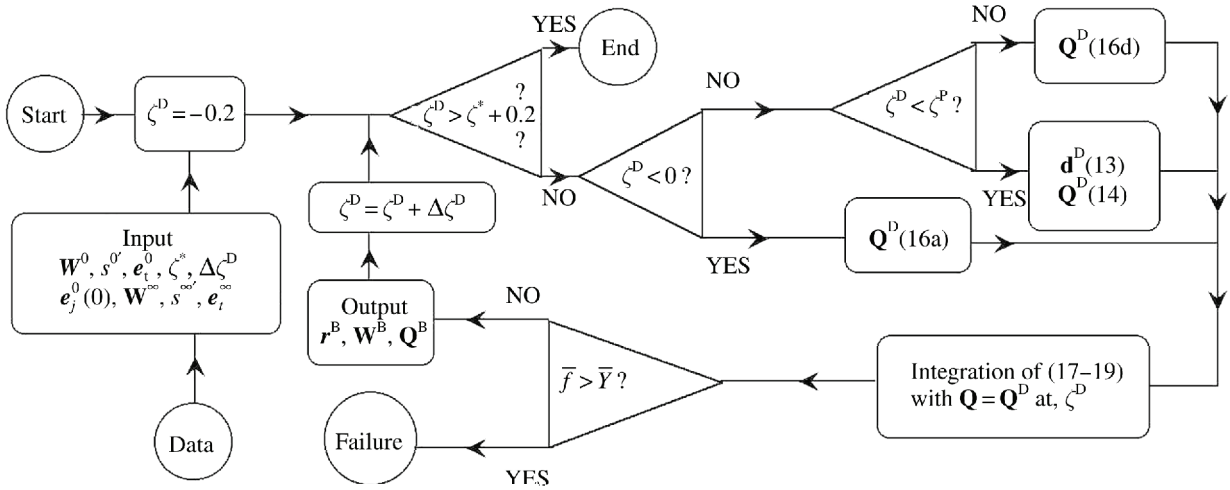

Fig. 2 Flow chart of the code for the finite strain approach without the Bernoulli hypothesis

initial state or to the terminal state rather than to previous steps. For this purpose, the meaning of the material coordinate ζ^D representing the position of the rear point of the plastic zone, D, will be generalized to become a dimensionless virtual time for the entire forming process. The integration may be carried out consecutively with the assumed number of discrete values of ζ^D. To this end, the forming process will be subdivided into three phases:

1. $-0.2 \leqslant \zeta^D < 0$, elastic/plastic pre-loading with $D \equiv A$.
2. $0 \leqslant \zeta^D \leqslant \zeta^*$, D moving from A to its final position D^* at which $\zeta^D = \zeta^* \leqslant \zeta^B$.
3. $\zeta^* < \zeta^D \leqslant \zeta^* + 0.2$, final elastic unloading with, $D \equiv D^*$.

The limit ± 0.2 has been chosen as arbitrary.

First of all, the limit stress $\mathbf{Q}^D = \mathbf{Q}^{DA} = [Q_{i'}^{DA}]^T$ has to be calculated for the left-hand support A by substituting the corresponding prescribed plastic strain $\mathbf{d}^{\infty A}$ into equation (14). Then the integration steps during phase 1 refer to the generalized stress

$$\mathbf{Q}^D = (1 + 5\zeta^D)\mathbf{Q}^{DA} \qquad \text{at } D = A \tag{16a}$$

and $\mathbf{Q}^D$ acts as the boundary value at D for the stress distribution to be determined below. As, in equation (16a), the proportional preloading may be replaced with any other preloading procedure, the deformation process is not unique during phase 1.

In phase 2 the assumed discrete values of ζ^D refer to different positions of D, where

$$\mathbf{d}^p = \mathbf{d}^\infty(\zeta^D) \qquad \text{at } \zeta = \zeta^D \text{ if } \zeta^A < \zeta^D \leqslant \zeta^* \tag{16b}$$

is prescribed while the corresponding stress $\mathbf{Q}^D$, acting again as the boundary value, follows from equation (14). This phase 2, most important for the forming process, is unique.

To each value of ζ^D the corresponding frontal point $P(\zeta = \zeta^P)$ of the plastic zone is determined, during phases 1 and 2, regarding equation (16b), by checking the solution of the differential equations to be formulated below with respect to the condition

$$\begin{aligned} &\mathbf{d}^p = \mathbf{0} \qquad \text{at } \zeta = \zeta^P \text{ provided } \zeta^D \leqslant \zeta^P < \zeta^B \text{ and} \\ &\qquad\qquad \mathbf{d}^\infty(\zeta^D) \neq \mathbf{0} \\ &P = B, \text{ i.e. } \zeta^P = \zeta^B \qquad \text{if } \mathbf{d}^p \neq \mathbf{0} \text{ for } \zeta^D < \zeta \leqslant \zeta^B \\ &P = D, \text{ i.e. } \zeta^P = \zeta^D \qquad \text{if } \mathbf{d}^\infty(\zeta^D) = \mathbf{0} \end{aligned} \tag{16c}$$

The loading process is finished after ζ^D has reached its final position, denoted by ζ^*. This coincides in most cases with ζ^B. However, it may be that the last section of the formed rod will remain undeformed. In this event, ζ^* is the value of ζ at the rear of that undeformed section, because, for reasons of continuity, $\mathbf{d}^\infty(\zeta^*) = \mathbf{0}$ has to be prescribed so that $P = D^*$ is found from the third equation of (16c). In the subsequent unloading phase 3, assumed to be elastic, the stress $\mathbf{Q}^{D*}$, belonging to D^*, will be reduced stepwise down to zero according to

$$\mathbf{Q}^D = \{1 + 5(\zeta^* - \zeta^D)\}\mathbf{Q}^{D*} \qquad \text{if } D \equiv D^* \tag{16d}$$

As this linear approach is arbitrary, unloading is not unique.

During the loading process in phases 1 and 2, the basic first-order differential equations for the generalized stress distribution $\mathbf{Q}$ consist of the equilibrium conditions (6) and (7) in which W_i and $s'e_i$ have been replaced with $d_{j'}(\mathbf{Q}) = d_{j'}(\mathbf{F}, \mathbf{M})$ via equations (5a) and (13) according to

$$F_k' + \varepsilon_{ijk}\{W_i^0 + s^{0\prime}\vartheta_i(\mathbf{F}, \mathbf{M})\}F_j + s^{0\prime}p_k = 0 \tag{17}$$

$$M'_k + \varepsilon_{ijk}\left(\left\{W_i^0 + s^{0\prime}\vartheta_i(\mathbf{F},\mathbf{M})\right\}M_j + \left\{s^{0\prime}e_i^0 + s^{0\prime}\varepsilon_i(\mathbf{F},\mathbf{M})\right\}F_j\right) + s^{0\prime}m_k = 0 \tag{18}$$

where p_k and m_k may generally be disregarded. At each time step these equations have to be integrated (numerically) along the rod under the boundary or end conditions (16a) to (16d), i.e. mutually with the geometric relations following from (2), (3) and (5) according to

$$\begin{aligned} e'_{j\lambda} &= \varepsilon_{ijk}\left(W_i^0 + s^{0\prime}\vartheta_i(\mathbf{F},\mathbf{M})\right)e_{k\lambda} \\ r'_\lambda &= e_{k\lambda}\left(s^{0\prime}\varepsilon_k(\mathbf{F},\mathbf{M}) + s^{0\prime}e_k^0\right) \qquad \text{if } \zeta \geqslant \zeta^{\mathrm{D}} \end{aligned} \tag{19}$$

Here, the initial conditions $\boldsymbol{r} = \mathbf{0}$ and $\boldsymbol{e}_j = \boldsymbol{e}_j^{\mathrm{A}0}$ at A have to be observed, $\boldsymbol{e}_j^{\mathrm{A}0}$ representing the initial values of the accompanying tripod. The elastic version of the above differential equations, defined in equations (12), has to be applied partly during phase 1, but always in front of D and during phase 3. In the latter event, i.e. during elastic unloading, equation (5b) has to be used rather than equation (5a) in order to set up (17) to (19), so that W_i^0 and $s^{0\prime}e_k^0$ have to be replaced with W_i^∞ and $s^{\infty\prime}e_k^\infty$ respectively. After each integration step, the static admissibility of the found stress solution has to be checked along the entire rod according to

$$\overline{f}(\mathbf{Q}) \leqslant \overline{Y}(\overline{d},\zeta) \tag{20}$$

where $\overline{d} = \overline{d}^0$ in front of P.

In any phase or at any time, the above differential equations deliver directly the position $\boldsymbol{r} = \boldsymbol{r}^{\mathrm{B}}$ and the corresponding orientation of the cross-section $\boldsymbol{e}_i = \boldsymbol{e}_i^{\mathrm{B}}$ for the end support B. These are the relevant control quantities of the system shown in Fig. 1.

Basically, the finite integration scheme described before may be applied, again incrementally, using the same equations, but now stepwise in a successive manner. The initial distributions (15) and $\overline{d}^0 = 0$ valid for the virgin rod have to be replaced, for any step, with the corresponding outcome of the foregoing step. Consequently, the stepwise numerical errors add up. Present practical experience shows that this is worse than the error due to the physically less correct finite approach.

4 BERNOULLI HYPOTHESIS

As a special approach sufficient for most applications, the Bernoulli hypothesis is often introduced, according to which $\overline{f}$ and f do not depend on $\mathbf{F}$ while

$$K_{j'l'} = 0 \qquad \text{if } j', l' = 4,5,6 \quad \text{so that } \varepsilon^{\mathrm{p}} \equiv \varepsilon^{\mathrm{e}} \equiv \mathbf{0} \tag{21}$$

Under assumption (15), this means that $\boldsymbol{e}_{\mathrm{t}} \equiv \boldsymbol{e}_1$ and $s \equiv s^0 \equiv s^\infty$ so that the cross-sections of the now inextensible rod are permanently orthogonal to the central trajectory. However, then the function g is no longer uniquely determined by f via equations (10); in particular, g may also depend in an arbitrary way on ε^{p}, or otherwise more or less arbitrary boundary conditions $\mathbf{F}^{\mathrm{D}}$ become possible for the normal and the shear forces acting on the cross-sections. Although these forces are of minor importance for the deformation of slender rods, they may effect failure of the forming process owing to re-plastification. In the examples below, no shear forces have been assumed at D, while the normal force was used tentatively to minimize the work generated at the supports.

5 EXAMPLES

Straight, untwisted rods from aluminium alloy AlMgSi 0.5 F22 (German standard designation, length $a^0 = 100$ mm) with rectangular cross-sections (3 mm × 10 mm in directions 2 and 3 respectively) have been formed by combined bending and torsion according to the prescribed, final state of deformation given in Fig. 3. The elastic moduli, i.e. $E = 65\,000\,\mathrm{N/mm^2}$ (Young's modulus) and $G = 24\,500\,\mathrm{N/mm^2}$ (shear modulus) as well as the moments of inertia of the cross-sections are known, so that the compliance coefficients, $K_{j'k'}$, could be formed regarding equations (21) in the usual manner. The torsion yield curve, $\overline{Y} = \overline{Y}(\overline{d})$, was determined experimentally; it can be approximated by the formula

$$\overline{Y}/\overline{Y}^0 = 1 + m\exp(n\overline{d}) \tag{22}$$

with $\overline{Y}^0 = 2.94\,\mathrm{N\,m}$, $m = 1.626$ and $n = 0.167$ mm, while

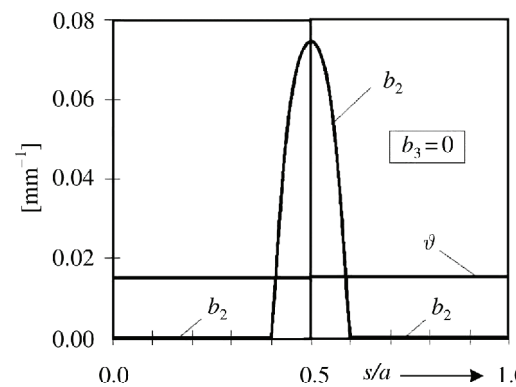

Fig. 3 Prescribed final deformation for a bent and twisted rod with bendings $b_2 = b_2^\infty$ and $b_3 = b_3^\infty$ and torsion $\vartheta = \vartheta^\infty$. Invariant arc length s and total length a

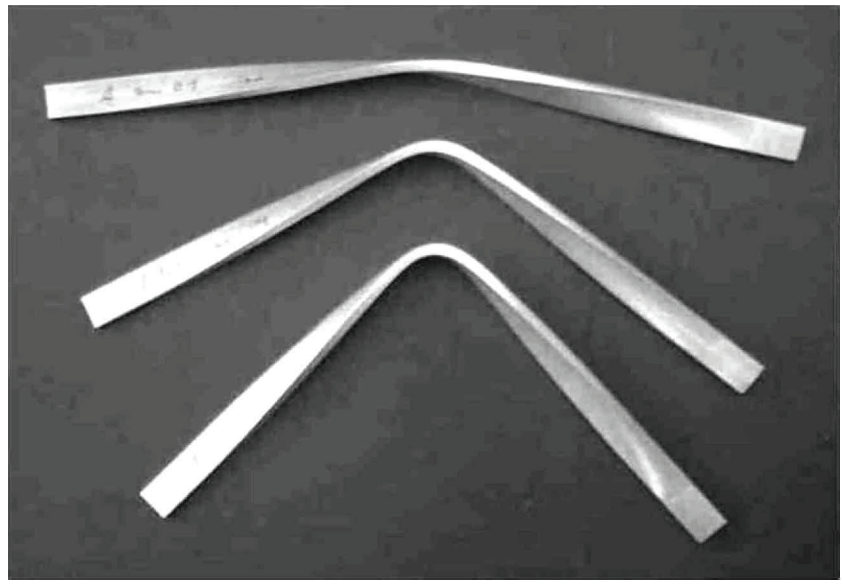

Fig. 4 Formed parts, the lower one corresponding to Fig. 2

the coefficients in the following Bernoulli-type approach

$$f = \overline{f} = \sqrt{\left(\frac{T}{\tau}\right)^2 + \left(\frac{M_2}{\mu_2}\right)^2 + \left(\frac{M_3}{\mu_3}\right)^2}$$
$$g = \sqrt{(\tau\vartheta^{\mathrm{p}})^2 + (\mu_2 b_2^{\mathrm{p}})^2 + (\mu_3 b_3^{\mathrm{p}})^2}, \qquad \tau = 1 \tag{23}$$

have been determined from simple bending or torsion tests, yielding

$$\mu_2 = \frac{M_{2\mathrm{L}}}{T_{\mathrm{L}}} = 0.9, \qquad \mu_3 = \frac{M_{3\mathrm{L}}}{T_{\mathrm{L}}} = 3.0 \tag{24}$$

where T_{L}, $M_{2\mathrm{L}}$ and $M_{3\mathrm{L}}$ are the plastic limit moments under torsion or bending. Then the parts shown in Fig. 4 have been obtained with a deviation from the prescribed position of less than 1 per cent of the free end B related to the rod length.

Moreover, applying approach (23), two conical spirals (cf. the Appendix) have also been formed from straight rods with initial lengths $a^0 = a = 759.5$ mm or 954.4 mm, using the same material as above, although with a circular cross-section (6 mm diameter) so that the yield curve parameters, i.e. $\overline{Y}^0 = 4.07\,\mathrm{N\,m}, m = 2.042, n = 0.168$ mm and $\mu_2 = \mu_3 = 0.98$, are different from those above. Actually, two or nearly three windings could be formed without re-plastification if the support A were chosen at the lowest radius (distance from the cone axis) $R = R^{\mathrm{A}}$ while B belonged to the largest radius $R = R^{\mathrm{B}}$. Remember that, at the cylindrical spiral, less than one winding was admissible {5}! Unfortunately, the forming accuracy of the conical spirals is worse, i.e. approximately 2 per cent rather than 1 per cent. The apex angle of the spirals ρ and the inclination angle α amounted to $\rho = 10^0$ and $\alpha = 10.151^0$ respectively. Then the angle $\overline{\alpha}$ projected on to a concentric cylinder of constant radius R, measured at the considered point of the spiral, would just amount to 10^0; this follows from $\tan(\overline{\alpha}) = \tan(\alpha)\cos(\rho)$ or, if $h = \text{constant}$, from $\tan(\overline{\alpha}) = h/(2\pi R)$. The minimal distances from the axis were $R^{\mathrm{A}} = 50$ mm for the shorter rod but $R^{\mathrm{A}} = 40$ mm for the longer rod. The distribution of the bending and torsion strains is given by equations (34) in the Appendix under the assumption that $b_2 = b_2^{\infty} \equiv W_2^{\infty}/s' \equiv 0$ {cf. equation (5a)} so that the first equation of (3) now becomes the Frenet equation of curve theory (cf. reference {7}) at which $\vartheta = \vartheta^{\infty} = W_1^{\infty}/s'$ equals the *mathematical torsion* θ of the central trajectory while $b_3 = b_3^{\infty} \equiv W_3^{\infty}/s'$ is the curvature κ. In the accompanying tripod, $\boldsymbol{e}_2$ and $\boldsymbol{e}_3$ point in the directions of the principal normal or of the binormal of the trajectory. Corresponding spirals have also been obtained experimentally; they are shown in Fig. 5.

6 CONCLUSIONS

By means of the forming process described in this paper, a great variety of slender plane or spatial parts can be produced with a good absolute, and an even better reproduction, accuracy. Limits are imposed by the uncontrollable re-plastification of already finished sections, provided the parts exceed a certain admissible length, or by buckling, not examined in this investigation. The forming process is flexible and inexpensive because it does not require any dies to be pre-manufactured. Also, the surface quality is excellent, although the production speed is still slow and the shape sensitivity to material defects is high.

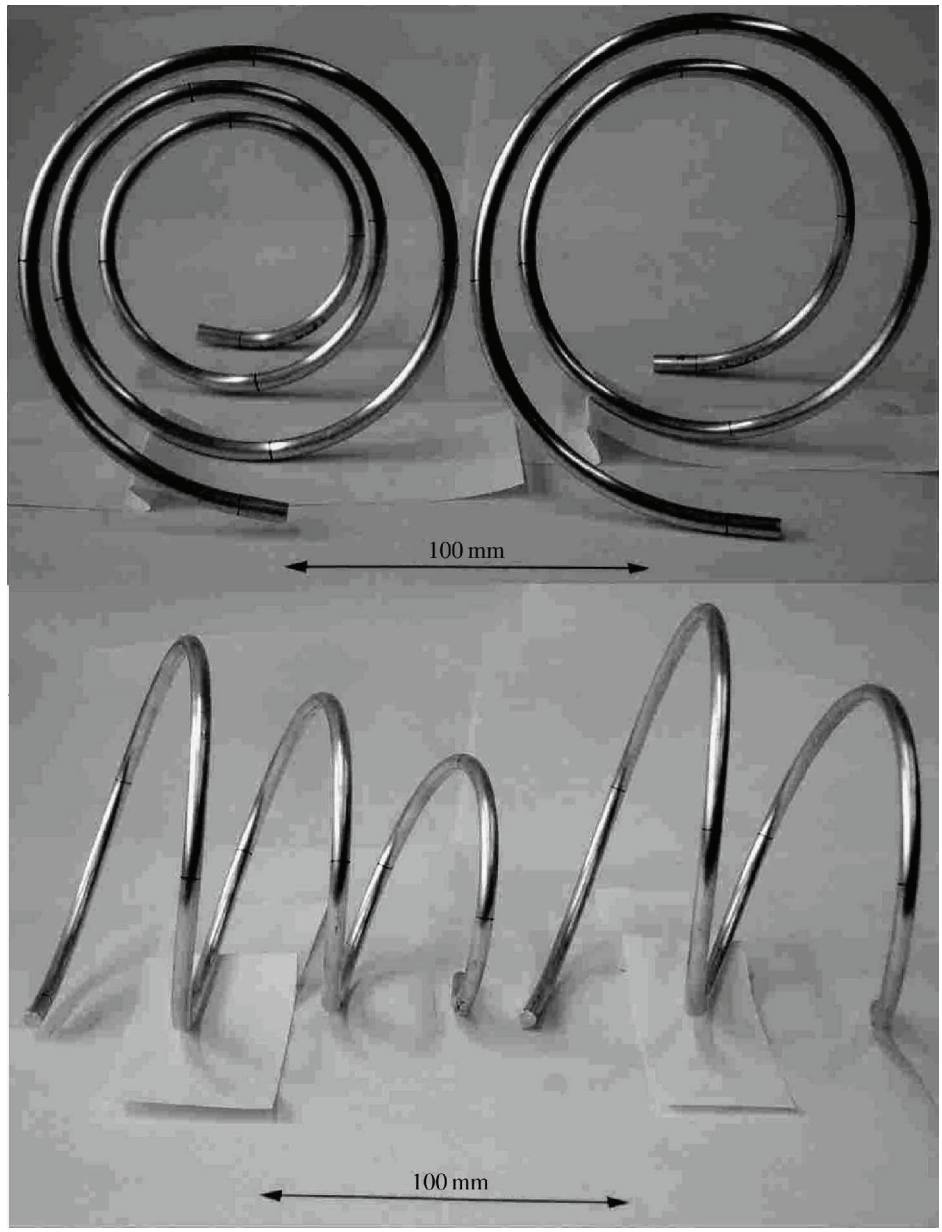

Fig. 5 Formed conical spirals with lengths $a = 759.5$ mm (right hand) and $a = 954.4$ mm (left hand)

ACKNOWLEDGEMENT

The financial support from the Deutsche Forschungsgemeinschaft (DFG) under Research Grant Li 115/44 is gratefully acknowledged.

REFERENCES

1 **Lippmann, H.** Free rigid/plastic bending of a slender beam. *Ing. Arch.*, 1990, **60**, 293–302.
2 **Reigl, M., Lippmann, H.** and **Mannl, V.** Erzeugung vielfältiger Werkstückformen durch kaltes und warmes endgesteuertes freies Biegen. In *Flexibel Umformtechnik*, Aachen, 1995, Section 2.2, pp. 1–15 (Deutsche Forschungsgemeinschaft, Wissenschaftsverlag, Mainz).
3 **Huang, X., Yu, T. X., Lu, G.** and **Lippmann, H.** Large deflection of elastoplastic beams under prescribed moving and rotating ends. *Proc. Instn Mech. Engrs, Part C: J. Mechanical Engineering Science*, 2003, **217**(C9), 1001–1013.
4 **Thalmair, M.** and **Lippmann, H.** Spatial free plastic forming of slender parts—fundamental relations and first example. *Int. J. Mech. Sci.*, 2000, **42**, 1851–1865.
5 **Thalmair, M., Lippmann, H.** and **Reigl, M.** Spatial free plastic forming of slender parts—machine design, forming limits, and application. *Trans. ASME, J. Engng Mater. Technol.*, 2001, **123**, 524–529.

6 Hill, R. Constitutive dual potentials in classical plasticity. *J. Mech. Phys. Solids*, 1987, **35**, 23–33.
7 Blaschke, W. *Introduction to Differential Geometry* (in German), 1950 (Springer-Verlag, Berlin, Germany).

APPENDIX

Conical spirals (Fig. 6)

Assuming $0 < \rho < 90°$, identifying ζ with the polar angle and introducing the distance from the central axis $R = R(\zeta)$ as a strictly monotonically growing smooth function obeying $R' > 0$, the coordinates of the central trajectory AB with respect to the base $\boldsymbol{e}_x, \boldsymbol{e}_y, \boldsymbol{e}_z$, fixed in space, are obtained by the corresponding projections of the position vector $\boldsymbol{r}(\zeta) = r_\lambda \boldsymbol{e}_\lambda$ according to

$$r_x = R(\zeta)\cos(\zeta), \qquad r_y = R(\zeta)\sin(\zeta)$$
$$r_z = R(\zeta)\tan^{-1}(\rho), \qquad \zeta^{\mathrm{A}} \leqslant \zeta \leqslant \zeta^{\mathrm{B}} \tag{25}$$

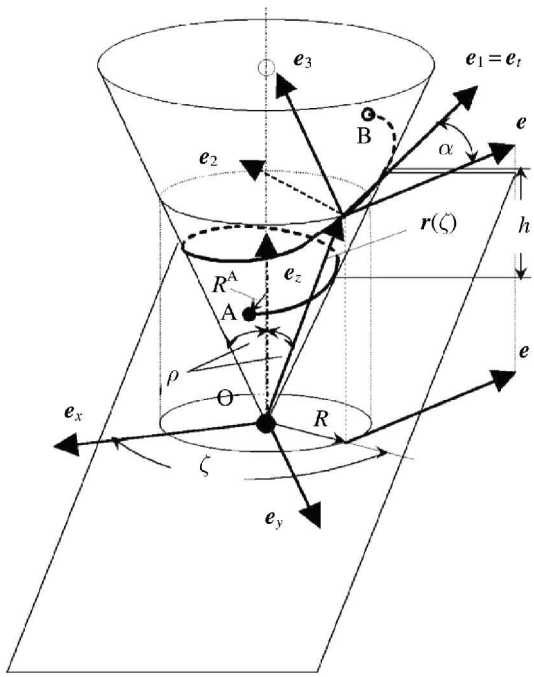

Fig. 6 Conical spiral AB defined on a virtual cone with apex semi-angle ρ, inclination α (measured tangentially to the cone) and lead h: $\boldsymbol{e}_1 = \boldsymbol{e}_t$ is the tangent to the spiral, $\boldsymbol{e}_2$ is the inward normal to the cone and $\boldsymbol{e}$ is the tangent to the horizontal circle on the cone, radius R

Consequently,

$$r'_x = R'\cos(\zeta) - R\sin(\zeta), \qquad r'_y = R'\sin(\zeta) + R\cos(\zeta)$$
$$r'_z = R'(\zeta)\tan^{-1}(\rho) \tag{26}$$

$$s' = \sqrt{(r'_x)^2 + (r'_y)^2 + (r'_z)^2} = \sqrt{[R'/\sin(\rho)]^2 + R^2} \tag{27}$$

Postulating the validity of the Bernoulli hypothesis and fixing the orientations of the cross-sections by means of the local tripod $\boldsymbol{e}_1, \boldsymbol{e}_2, \boldsymbol{e}_3$ temporarily so that $\boldsymbol{e}_2$ is an inward normal to the cone, the unit tangent to the trajectory, $\boldsymbol{e}_1 = \boldsymbol{e}_t$, is obtained from equations (2). Being orthogonal to $\mathrm{e_t}$ as well as to any other tangent of the cone, such as $\boldsymbol{r}$, the inward normal $\boldsymbol{e}_2$ must obey $\boldsymbol{e}_1\boldsymbol{e}_2 = 0, \boldsymbol{e}_2\boldsymbol{e}_2 = 1, \boldsymbol{r}\boldsymbol{e}_2 = 0$ and $\boldsymbol{e}_z\boldsymbol{e}_2 > 0$. This is fulfilled by the unit vectors

$$\boldsymbol{e}_1 = \frac{1}{s'}\left(r'_x\boldsymbol{e}_x + r'_y\boldsymbol{e}_y + r'_z\boldsymbol{e}_z\right)$$
$$\boldsymbol{e}_2 = -\cos(\rho)\left(\cos(\zeta)\boldsymbol{e}_x + \sin(\zeta)\boldsymbol{e}_y\right) + \sin(\rho)\boldsymbol{e}_z$$
$$\boldsymbol{e}_3 = \boldsymbol{e}_1 \times \boldsymbol{e}_2 = \frac{1}{s'}\left\{\left[R'\frac{\sin(\zeta)}{\sin(\rho)} + R\cos(\zeta)\sin(\rho)\right]\boldsymbol{e}_x + \left[-R'\frac{\cos(\zeta)}{\sin(\rho)} + R\sin(\zeta)\sin(\rho)\right] \times \boldsymbol{e}_y + R\cos(\rho)\boldsymbol{e}_z\right\} \tag{28}$$

Moreover, using equations (27) and (28) it is seen that

$$\boldsymbol{e} = -\sin(\zeta)\boldsymbol{e}_x + \cos(\zeta)\boldsymbol{e}_y, \qquad \cos(\alpha) = \boldsymbol{e}$$
$$\boldsymbol{e}_1 = \frac{R}{s'}$$
$$\sin(\alpha) = \sqrt{1 - \left(\frac{R}{s'}\right)^2} - \sin(\alpha)\alpha' = \frac{R'}{s'} - \frac{Rs''}{(s')^2}$$
$$\alpha' = \left(\frac{R}{R'}\frac{s''}{s'} - 1\right)\sin(\rho) \tag{29}$$

Moving along the trajectory by the *virtual time* increment $\mathrm{d}\zeta$ causes *virtual rotation* of the cross-section, $\mathbf{W}\,\mathrm{d}\zeta$, to occur. For the special cross-sectional orientation of Fig. 6, this consists of the polar rotation $\mathrm{d}\zeta$ around the z axis and of a subsequent rotation $\mathrm{d}\alpha$ around the negative normal to the cone, $-\boldsymbol{e}_2$, so that expressing the unit vector $\boldsymbol{e}_z$ in terms of $\boldsymbol{e}_j$ and observing equations (28)

$$\mathbf{W} = \boldsymbol{e}_z - \alpha'\boldsymbol{e}_2 = (\boldsymbol{e}_z\boldsymbol{e}_j)\boldsymbol{e}_j - \alpha'\boldsymbol{e}_2$$
$$= \frac{R'}{s'}\tan^{-1}(\rho)\boldsymbol{e}_1 + [\sin(\rho) - \alpha']\boldsymbol{e}_2 + \frac{R}{s'}\cos(\rho)\boldsymbol{e}_3 \tag{30}$$

Now consider other orientations of the cross-sections. For these, axes 2 and 3 are rotated around the tangent $\boldsymbol{e}_1$ by a possibly variable angle $\varphi = \varphi(\zeta)$, generating the virtual rotation $\varphi' \, \mathrm{d}\zeta$. Therefore, $\mathbf{W}$ has to be replaced with $\mathbf{W} + \varphi' \boldsymbol{e}_1$, while coordinates 2 and 3 of $\mathbf{W}$ must be transformed into rotated directions 2 and 3 according to $W_2 \cos(\varphi) + W_3 \sin(\varphi)$ and $-W_2 \sin(\varphi) + W_3 \cos(\varphi)$. Consequently, with account taken of equation (30) the new coordinates of $\mathbf{W}$ become

$$
\begin{aligned}
W_1 &= \frac{R'}{s'} \tan^{-1}(\rho) + \varphi' \\
W_2 &= [\sin(\rho) - \alpha'] \cos(\varphi) + \frac{R}{s'} \cos(\rho) \sin(\varphi) \\
W_3 &= -[\sin(\rho) - \alpha'] \sin(\varphi) + \frac{R}{s'} \cos(\rho) \cos(\varphi)
\end{aligned}
\tag{31}
$$

In particular, for the Frenet tripod {7}, the components of $\mathbf{W}$ have the form

$$
\begin{aligned}
&\frac{W_1}{s'} = \theta \ \text{(mathematical torsion)}, \qquad W_2 = 0 \\
&\frac{W_3}{s'} = \kappa \ \text{(curvature)}
\end{aligned}
\tag{32}
$$

{cf. equations (5)}. Here, with account taken of equations (31), the generic condition, i.e. the second equation of (32), leads to

$$
\begin{aligned}
\tan(\varphi) &= \frac{s'}{R} \frac{\alpha' - \sin(\rho)}{\cos(\rho)} \\
\varphi' &= \frac{\tan(\varphi)}{1 + \tan^2(\varphi)} \left[\frac{s''}{s'} - \frac{R'}{R} + \frac{\alpha''}{\alpha' - \sin(\rho)} \right]
\end{aligned}
\tag{33}
$$

Finally, the special case $\alpha = \text{constant}$ will be addressed. Here, with account taken of equations (31) and (32), equations (26) and (27) deliver $R'/R = \tan(\alpha) \sin(\rho)$ so that

$$
\begin{aligned}
R &= R^{\mathrm{A}} \exp\left[(\zeta - \zeta^{\mathrm{A}}) \tan(\alpha) \sin(\rho) \right] \\
s' &= \frac{R}{\cos(\alpha)}, \qquad s = \frac{R - R^{\mathrm{A}}}{\sin(\alpha) \sin(\rho)} \\
\tan(\varphi) &= -\frac{\tan(\rho)}{\cos(\alpha)} = \text{constant} \\
W_1 &= \theta s' = \sin(\alpha) \cos(\rho) = \text{constant} \\
W_2 &\equiv 0 \\
W_3 &= \kappa s' = -\sin(\rho) \sin(\varphi) + \cos(\alpha) \cos(\rho) \cos(\varphi) \\
&= \text{constant}
\end{aligned}
\tag{34}
$$